Source of magnetic anisotropy in quasi-two-dimensional XY {Cu$_4$(tetrenH$_5$)W(CN)$_8$]$_4$·7.2H$_2$O)}$_n$ bilayer molecular magnet

O. Zaharko,[1] M. Pregelj,[1,2] A. Zorko,[2,3] R. Podgajny,[4] A. Gukasov,[5] J. van Tol,[6] S. I. Klokishner,[7] S. Ostrovsky,[7] and B. Delley[8]

[1]*Laboratory for Neutron Scattering, Paul Scherrer Insitute, CH-5232 Villigen, Switzerland*
[2]*Jožef Stefan Institute, Jamova 39, SI-1000 Ljubljana, Slovenia*
[3]*EN-FIST Centre of Excellence, Dunajska 156, SI-1000 Ljubljana, Slovenia*
[4]*Faculty of Chemistry, Jagiellonian University, Ingardena 3, 30-060 Kraków, Poland*
[5]*Laboratoire Léon Brillouin, CEA-SNRS, CE Saclay, 91191 Gif sur Yvette, France*
[6]*National High Magnetic Field Laboratory, Florida State University, Tallahassee, Florida 32310, USA*
[7]*Institute of Applied Physics, Academy of Sciences of Moldova, MD-2028 Chisinau, Republic of Moldova*
[8]*Condensed Matter Theory, Paul Scherrer Insitute, CH-5232 Villigen, Switzerland*

To identify the origin of the XY spin dimensionality in the bilayered system {Cu$_4$(tetrenH$_5$)[W(CN)$_8$]$_4$·7.2H$_2$O}$_n$ (WCuT) we use a combination of single-crystal experiments (bulk magnetization, neutron flipping ratio, electron magnetic resonance, neutron diffraction) and theoretical modeling (exchange-charge model of the crystal field, dipolar energy, and density functional calculations). Our experiments show that the magnetic properties of WCuT are anisotropic and two-dimensional correlations build up below 70 K. The hard anisotropy axis is perpendicular to the layers (b axis) and a small anisotropy within the ac layers is present. Modeling of the crystal field validates treatment of tungsten and copper as spin $S = \frac{1}{2}$ ions with anisotropic g values. The local magnetic anisotropy results from the common action of the crystal field and spin-orbit coupling and is along the c axis for both ions. Density functional calculations identify the origin of the ferromagnetic exchange in different energies and symmetries of the tungsten- and copper-dominated orbitals and anticipate different exchange couplings across the apical (along the b axis) and equatorial (in the ac plane) Cu-CN-W bridges due to difference in the hybridization efficiency. Calculation of the dipolar energy for various spin configurations suggests that dipolar interactions play a decisive role in the ac-planar anisotropy in this system. We propose that the effective XY spin dimensionality in WCuT is established by a combination of the axial local anisotropy of the W and Cu ions and the long-range magnetic dipolar interactions on the bilayered square lattice.

I. INTRODUCTION

Reduction of *spatial* extension from three (3D) to two (2D) dimensions offers new physical phenomena relevant to superconductivity, superfluidity, and quantum magnetism and is of potential technological importance.[1–3] In magnetic materials such spatial reduction might also cause low *spin* dimensionality. In the genuine XY model[4,5] only two spin components S^x and S^y ($N = 2$) are involved and arising magnetic properties are described by the effective Hamiltonian:[6,7]

$$H = J \sum_{i,j} \left(S_i^x S_j^x + S_i^y S_j^y \right). \tag{1}$$

The unique feature of the XY model is the topological Berezinskii-Kosterlitz-Thouless (BKT) transition,[4,5] which is caused by specific 2D excitations, vortices.

Two-dimensional materials may behave like 2D Heisenberg [e.g., La$_2$CuO$_4$ (Ref. [8])], XY [e.g., K$_2$CuF$_4$ (Refs. [9] and [10])], or Ising [e.g., Rb$_2$CoF$_4$ (Ref. [11])] spin systems. Small anisotropies in a layer and weak coupling between layers drive real 2D materials to long-range 3D magnetic order. Yet often these transitions maintain the main features of the Kosterlitz-Thouless transition. Usually two main sources of magnetic anisotropy, "local" and "long-range," are distinguished.[12] To discriminate between the two is often difficult, as they emerge from various aspects of electron exchange and spin-orbit interactions. Local anisotropy is dominated by one magnetic center and its surroundings, while long-range anisotropy arises from the interaction of several magnetic centers, that is, anisotropy of intersite exchange and of dipolar interactions.

In this work we identify the origin of magnetic anisotropy in the quasi-2D XY magnet copper-octacyanotungstenate {Cu$_4$(tetrenH$_5$)[W(CN)$_8$]$_4$·7.2H$_2$O}$_n$ (tetren = tetraethylenepentaamine), hereafter abbreviated WCuT. This compound, first reported by Podgajny *et al.*,[13] crystallizes in the non-centrosymmetric $Cmc2_1$ ($a = 7.379$ Å, $b = 32.096$ Å, $c = 7.016$ Å) structure and consists of anionic bilayers stacked along the b axis. The Cu^{II} ($3d^9$, $S = \frac{1}{2}$) and W^V ($5d^1$, $S = \frac{1}{2}$) ions occupy the individual $4a$ Wyckoff sites and are joined by the network of cyanobridges (Fig. 1). Four *equatorial* cyanide CN$^-$ bridges give rise to the square grid pattern of the single layer, while the *apical* CN$^-$ bridges join two layers into the bilayer.[14] The structure is stabilized by the tetrenH$_5^{5+}$ cations, which counterbalance the negative charge of the bilayers and, together with water molecules, fill the interlayer space in a disordered fashion.

Magnetic properties of WCuT studied earlier on polycrystalline and single-crystal samples[13–17] reveal quasi 2D behavior. Analysis of the μSR results and magnetic susceptibility[16,17] in terms of scaling behavior and critical exponents indicated the XY character of the transition at T_C and its underlying BKT nature.[16,17] The exchange interactions within the bilayers are ferromagnetic (FM), while the weak coupling between the bilayers is antiferromagnetic (AF) and possibly of dipolar origin.[17] Three-dimensional long-range AF
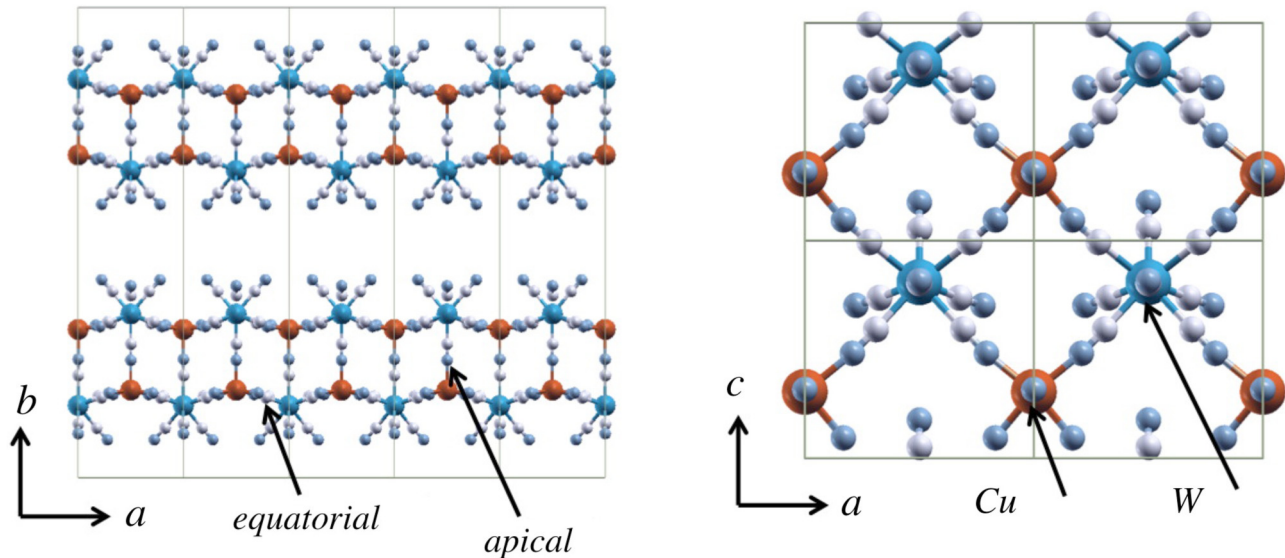
FIG. 1. (Color online) (Left) Arrangement of bilayers in WCuT (Ref. 13). The W atoms are shown by blue; Cu, orange; N, light blue; C, gray. The disordered cation layer is not shown. (Right) The square-grid pattern of a single layer.

ordering occurs below $T_C = 34$ K[13] in zero magnetic field. Below T_C the magnetization is strongly anisotropic, it is nearly one order of magnitude larger in the ac plane than in the out-of-plane direction, parallel to the b axis.[17] The average FM intra-bilayer exchange coupling is estimated as $J = -77.5$ K, while the AF inter-bilayer coupling only $J' = 7.5$ mK;[17] this results in $|J'/J| \approx 10^{-4}$. A small magnetic field of 50 G applied in the ac plane induces a metamagnetic transition from the AF state to a FM ordered state[15]; thus, the ac plane is the magnetic easy plane.

We examined the magnetic anisotropy of the WCuT system by bulk magnetization, electron magnetic resonance (EMR) spectroscopy, polarized neutron flipping ratio (FR), and nonpolarized neutron diffraction on single crystals. The experimental information is complemented by exchange-charge modeling of the crystal field (CF), calculation of the energy of dipolar interactions, and density functional (DFT) calculations. We suggest that the XY dimensionality of the system evolves from the (c-) axial local anisotropy of the g factors of both constituent magnetic ions, Cu^{II} and W^V, which acquires the (ac-) planar character due to the long-range dipolar interactions occurring in the WCuT lattice with predominantly isotropic FM exchange.

II. EXPERIMENTAL

A. Electron magnetic resonance measurements

Measurements of the bulk dc magnetization on our crystals are in accord with the results reported earlier.[17] The magnetization deviates from the Curie-Weiss law below 150 K and the Curie-Weiss temperature agrees with the published values of $\theta = 43.5$ K for a polycrystalline sample[13] and $\theta_{ac} = 53.7$ K, $\theta_b = 51.0$ K for a single crystal.[17] To study further the anisotropy of the response of WCuT crystals to magnetic field we performed EMR measurements using a home-built resonator-based spectrometer in the X band (9.38 GHz) and a custom-made reflection spectrometer at 120 and 239.2 GHz

at the National High Magnetic Field Laboratory in Tallahasee, FL. A very broad signal is observed below 100 K, whose width increases with increasing temperature. Consequently, a reliable analysis of the signal could be performed only below 70 K. The fact that a single resonant line is found at all frequencies (9.38, 120, and 239.2 GHz) suggests that either one of the two spin-$\frac{1}{2}$ magnetic species (W^V and Cu^{II}) is EMR silent, or that strong exchange coupling between the two leads to a single exchange-narrowed line. The signal exhibits strongly anisotropic behavior at all temperatures. The linewidth ΔB and the resonant field $B_{\rm res}$ are substantially different for magnetic fields applied along the b axis and perpendicular to it (Fig. 2, left), while both parameters are almost angle-independent in the ac plane. The angular anisotropy of the linewidth and the line shift with respect to $B_0 = \frac{h\nu}{g_0\mu_B}$ ($g_0 = 2.0023$ is the free-electron g factor, h the Planck constant, and μ_B the Bohr magneton) are found to be strongly temperature dependent (Fig. 2, right). The temperature-dependent line shift is frequency independent, as seen from comparison of 120 and 239.2 GHz data in Fig. 2(a). Therefore, this cannot be a result of changes in the g factor. Rather it reveals the presence of internal magnetic fields, which are static on the EMR time scale. This is somewhat unusual, as shifts are observed at least up to 70 K, that is, far above the 3D ordering temperature T_N. Thus, spin correlations, presumably of 2D nature, are present already at high temperatures. The nonparamagnetic behavior of the EMR signal is also evident from the frequency-field diagram, shown in Fig. 3 for 45 K. The lines connecting the high-frequency points clearly do not extrapolate to the origin and thus reveal a finite zero-field splitting, indicating a gap in the magnetic excitations. Such behavior is characteristic of collective excitations.[18] Due to this magnon scattering the linewidth usually increases with increasing temperature, and indeed such behavior is experimentally observed in Fig. 2(b). The gap opens progressively, as indicated by the gradual shift of the line with temperature. From the slopes in Fig. 3 we estimate the g-factor values $g_b = 1.91$ and $g_c = 2.18$. This
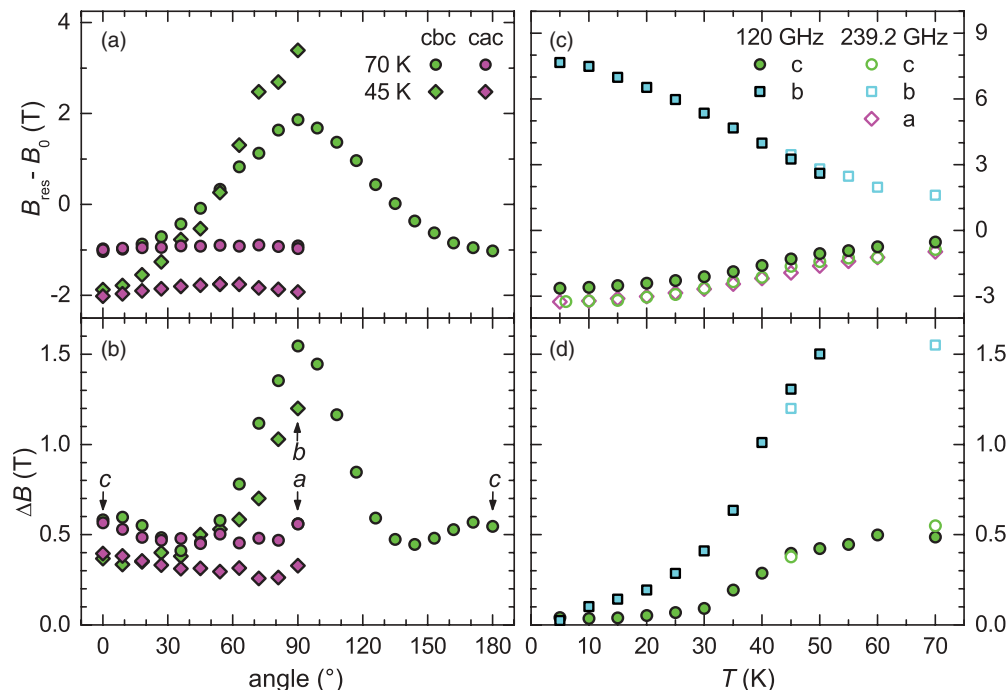
FIG. 2. (Color online) (Left) Angular dependence of EMR (a) line shift and (b) linewidth (with respect to $B_0 = \frac{h\nu}{g_0\mu_B}$, $\nu = 239.2$ GHz) at 70 K and 45 K. Labels *cbc* and *cac* refer to the sense of field rotation relative to the principal crystallographic directions. (Right) Temperature dependence of EMR (c) line shift and (d) linewidth.

suggests a combined Cu/W excitation, as typical g values for W^V are below g_0 (Ref. 19) and for Cu^{II} above g_0 (Ref. 20) (also see Sec. III A).

B. Internal magnetic field tensors from neutron flipping ratios

To differentiate the magnetization distributions around the W^V and Cu^{II} ions we performed a neutron FR experiment. The FR R is defined as the ratio of diffracted intensities of neutrons polarized parallel I_+ and antiparallel I_- to the

FIG. 3. (Color online) Frequency-field diagram measured at 45 K.

external magnetic field:

$$R = \frac{I_+}{I_-} = \frac{|F_N|^2 + \mathbf{P} \cdot \mathbf{F}_M^\perp F_N^* + \mathbf{P} \cdot \mathbf{F}_M^{\perp *} F_N + |\mathbf{F}_M^\perp|^2}{|F_N|^2 - \mathbf{P} \cdot \mathbf{F}_M^\perp F_N^* - \mathbf{P} \cdot \mathbf{F}_M^{\perp *} F_N + |\mathbf{F}_M^\perp|^2}. \quad (2)$$

Here $\mathbf{P}$ is the neutron polarization vector, $\mathbf{F}_M^\perp$ is the magnetic interaction vector defined by $\mathbf{F}_M^\perp(\mathbf{k}) = \mathbf{k} \times \mathbf{F}_M(\mathbf{k}) \times \mathbf{k}$, and $\mathbf{k}$ is the scattering vector. If the nuclear structure factors are known (F_N is the real part and F_N^* is the imaginary part), the magnetic structure factors $\mathbf{F}_M$ can be extracted. The magnetic structure factors are complex vectors and are given by

$$\mathbf{F}_M(\mathbf{k}) = \Sigma_a f_a(\mathbf{k}) \Sigma_\mathbf{k} \mathbf{M}_a(\mathbf{r}_a) e^{i\mathbf{k}\mathbf{r}_a}, \quad (3)$$

where $f_a(\mathbf{k})$ is the magnetic form factor, $\mathbf{M}_a(\mathbf{r}_a)$ is a vector representing the magnetic moment, and $\mathbf{r}_a$ is a vector defining the position of the ath atom in the unit cell. The sum $\Sigma_\mathbf{k}$ extends over all reciprocal vectors $\mathbf{k}$ and the sum Σ_a over all atoms in the unit cell. The magnetic moments of individual atoms can be extracted as a Fourier transform of the magnetic structure factors.

The total magnetization $\mathbf{M}_i$ induced in a material by a magnetic field $\mathbf{H}_j$ can be approximated by the vector sum of magnetic moments on constituent magnetic atoms (i, j are spatial coordinates). The response of each individual atom λ_{ij} is

$$\mathbf{M}_i = \Sigma_j \lambda_{ij} \mathbf{H}_j. \quad (4)$$

This response is, in general, anisotropic and depends on the local symmetry of a magnetic ion.[21–23] In an ideal paramagnet (i.e., the Curie-Weiss law is obeyed) λ_{ij} is identical to the susceptibility tensor χ_{ij}. In a nonideal paramagnet (i.e., correlations among magnetic moments are strong) it is more appropriate to refer to an anisotropic molecular field tensor

TABLE I. Details of the neutron FR experiment and refined components of the AMFT tensors of the Cu^{II} and W^V ions (in μ_B/T) (Ref. 28).

| T (K) | N_{ref} | | | W^V | | | | | Cu^{II} | | | | |
	a'	b	c	λ_{aa}	λ_{bb}	λ_{cc}	$\lambda_{aa}/\lambda_{cc}$	$\lambda_{bb}/\lambda_{cc}$	λ_{aa}	λ_{bb}	λ_{cc}	$\lambda_{aa}/\lambda_{cc}$	$\lambda_{bb}/\lambda_{cc}$
70	83	35	13	0.022(3)	0.01(2)	0.029(4)	0.76(15)	0.3(7)	0.036(2)	0.02(1)	0.027(2)	1.33(12)	0.7(5)
45	74	44	33	0.062(3)	0.04(1)	0.077(2)	0.81(4)	0.5(1)	0.104(3)	0.08(1)	0.084(4)	1.24(7)	1.0(3)
2	85	72	32	0.114(3)	0.06(2)	0.138(7)	0.83(5)	0.44(3)	0.189(3)	0.15(1)	0.148(4)	1.28(4)	1.01(7)

(AMFT) λ_{ij}, as it represents a combined response to external and internal magnetic fields.

The FR experiment was performed on the 6T2 diffractometer at the Orphée reactor of the Laboratoire Léon Brillouin, France. Neutrons of the wavelength 1.4 Å from the PG monochromator were vertically polarized by a supermirror bender and flipped by an adiabatic radio-frequency flipper. A 9-mg crystal was mounted in a superconducting magnet and a vertical magnetic field of 6 T was applied. Measurements at 70 K, 45 K, and 2 K were done in the three orientations: the magnetic field was applied along the a', b, and c axes.[24] The number of collected reflections was limited, with the smallest dataset obtained for H$||c$. To extract the magnetic structure factors $\mathbf{F}_M$ we used the nuclear structure factors F_N from the structural refinement of the nonpolarized neutron diffraction data collected on the TriCS single-crystal diffractometer at the spallation neutron source SINQ, Paul Scherrer Institute, Switzerland. The refinement of the induced magnetization and of the corresponding AMFT tensors was performed by the CHILSQ program from the CCSL package.[25] The spherical magnetic form factors for Cu^{II} and W^V were used.[26,27]

The symmetry of the individual AMFT tensors of the Cu^{II} and W^V ions is the same as that of the tensors describing the thermal motion of the atoms. For the WCuT crystal structure they have the following form:

$$\lambda_{ij} = \begin{vmatrix} \lambda_{aa} & 0 & 0 \\ 0 & \lambda_{bb} & \lambda_{bc} \\ 0 & \lambda_{cb} & \lambda_{cc} \end{vmatrix}, \qquad (5)$$

with $\lambda_{bc} = \lambda_{cb}$. The components λ_{aa}, λ_{bb}, λ_{cc} correspond to the a, b, and c axes, respectively. The components of the AMFT tensors obtained by combined refinement of the three orientations for each temperature are presented in Table I. The AMFT tensor of W is more anisotropic than that of Cu. Thus, the contribution of tungsten to the observed magnetic anisotropy is larger. As expected, the ratios of the components of AMFTs $\lambda_{aa}/\lambda_{cc}$ and $\lambda_{bb}/\lambda_{cc}$ remain constant with decreasing temperature within the accuracy of our data, while the absolute values increase with decreasing temperature in accordance with the measured bulk susceptibility.

Combining all FRs collected at 2 K, we calculated the magnetic density distribution using the maximum entropy method implemented in the program PRIMA.[29] Figure 4 presents the *ab* projection of magnetization density obtained by this model-free approach. The dominant part of magnetic density is distributed on the copper and tungsten atoms in the layer as follows from the AMFT approach. However, additional details can be observed: the density near the Cu atom is elongated towards the neighboring equatorial

nitrogen and the density near W spreads to the terminal CN$^-$ groups, which are located towards distorted cation interlayers. These observations agree with the results of DFT calculations presented in Sec. III B.

C. Low-temperature magnetic structure by neutron diffraction

Our experimental results and Ref. 17 show that the *ac* plane is the easy magnetic anisotropy plane. To investigate the anisotropy within this plane and to determine the ground state of WCuT we performed a nonpolarized neutron single-crystal diffraction experiment. The measurement in zero field was performed on the TriCS diffractometer using the PG monochromator (wavelength 2.32 Å) and a cooling machine mounted on a four-circle cradle with the same WCuT crystal as for the FR experiment. At 6 K eight magnetic reflections indexed with the wave vector $\mathbf{k} = (100)$ were measured. For the given wave vector and the space group, four irreducible representations (IRRs) are possible for the 4a Wyckoff site describing the local symmetry of copper and tungsten. The Fourier components of the corresponding four magnetic structures are listed in Table II. The best agreement with the observed intensities is obtained for $M_z = 0.91(7)$ μ_B component of the Γ_3 representation. Due to the limited experimental data we had to assume the same magnetic moment at the Cu and W sites. For the same reason, we cannot determine the M_y component which would exist if the Dzyaloshinsky-Moria (DM) interactions[30] are present. According to the symmetry of the WCuT crystal structure the DM vector should be perpendicular to m_x planes which pass through the apical Cu-NC-W pathways.

In the best refined model all magnetic moments within the bilayer are parallel, as expected for a strong FM intralayer
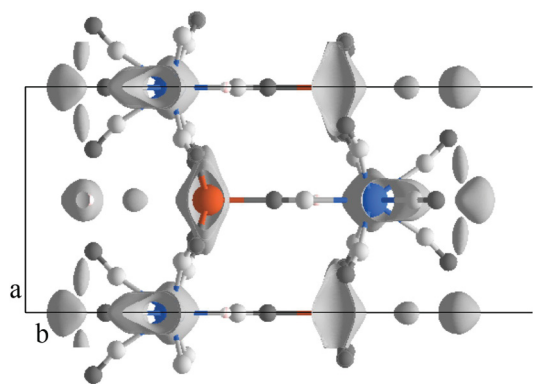
FIG. 4. (Color online) The *ab* projection of magnetization density (gray isosurface) obtained from maximum entropy reconstruction of the FRs collected at 2 K. The color code of atoms of Fig. 1 is adopted.

TABLE II. Fourier components M_x, M_y, M_z of the symmetry allowed magnetic structures.

		Atom 1: (x,y,z)			Atom 2: $(-x,-y,z+1/2)$	
Γ_1	M_x	0	0	$-M_x$	0	0
Γ_2	0	M_y	M_z	0	$-M_y$	M_z
Γ_3	0	M_y	M_z	0	M_y	$-M_z$
Γ_4	M_x	0	0	M_x	0	0

interaction and are pointing along the c axis. On the other hand, the spins in the neighboring bilayers are antiparallel, signifying AF coupling (J') between the bilayers. During the metamagnetic transition at $B_{ac} = 50$ G the Zeeman energy exceeds the inter-bilayer coupling ($g\mu_B B_{ac} = 2zJ'S$) and the magnetic moment of every second bilayer reverses, resulting in a FM structure.

III. THEORETICAL MODELING

A. Exchange-charge model of the crystal field for the W^V and Cu^{II} ions

To model the local anisotropy we performed a calculation of the Stark structure of the ground terms of the W^V and Cu^{II} using an exchange-charge model of the CF. In this model the parameters B_l^m of the CF operator

$$V_{cr} = \Sigma_{l,m} B_l^m Y_l^m(\theta,\phi), \qquad (6)$$

where $Y_{l,m}(\theta,\phi)$ are the spherical harmonics, account for two contributions,[31,32]

$$B_l^m = B_l^{m(pc)} + B_l^{m(ec)}, \qquad (7)$$

where the component

$$B_l^{m(pc)} = \frac{4\pi}{2l+1} \Sigma_\alpha \frac{Z_\alpha e^2 \langle r \rangle^l}{(R_\alpha)^{l+1}} Y_l^{m*}(\theta_\alpha,\phi_\alpha) \qquad (8)$$

is determined as in Refs. 31 and 32. The point charge contribution $B_l^{m(pc)}$ depends on the positions of the ligands (R, θ, ϕ are the spherical coordinates of the ligand), their effective charges Z_α (value -1 is taken for the CN ligands), and radial integrals $\langle r^2 \rangle = 2.52a_0^2$ and $\langle r^4 \rangle = 9.3a_0^4$ for the tungsten ions[33] and $\langle r^2 \rangle = a_0^2$ and $\langle r^4 \rangle = 2.1a_0^4$ for the copper ions;[34] a_0 is the Bohr radius. The contribution $B_l^{m(ec)}$,

$$B_l^{m(ec)} = \frac{8\pi e^2}{5} G \Sigma_\alpha \frac{S_l(R_\alpha)}{R_\alpha} Y_l^{m*}(\theta_\alpha,\phi_\alpha), \qquad (9)$$

is proportional to a linear combination of squares of different type overlap integrals of the $5d$ functions of the W^V ions and the $2s$, $2p$ wave functions of the carbons in the case of tungsten and the $3d$ functions of the Cu^{II} ions and the $2s$, $2p$ wave functions of the nitrogens in the case of copper,

$$S_p(R_\alpha) = S_s^2(R_\alpha) + S_\sigma^2(R_\alpha) + \gamma_p S_\pi^2(R_\alpha),$$
$$\gamma_2 = 1, \quad \gamma_4 = -4/3, \qquad (10)$$

where $S_s(R_\alpha) = \langle nd, m = 0|2s \rangle$, $S_\sigma(R_\alpha) = \langle nd, m = 0|2p, m = 0 \rangle$, and $S_\pi(R_\alpha) = \langle nd, m = \pm 1|2p, m = \pm 1 \rangle$ are the overlap integrals of the nd wave functions of tungsten[35] or copper[36] ions and $2s$, $2p$ wave functions of the C or N ligands[36] and G is the phenomenological parameter of the model. For tungsten ions the value of this parameter is estimated from the expression

$$Dq = -\frac{4(5e^2\langle r^4 \rangle Z + 18e^2 R^4 G S_4(R))}{135 R^5}. \qquad (11)$$

For the average values $R = 2.61$ Å and $S_4(R) = 0.07798$ and the CF parameter $Dq = 3380$ cm^{-1} from Ref. 37 we obtained $G = 1.39$. The CF potential for the W^V ion in the bicapped trigonal prism ligand surrounding has the form

$$\begin{aligned}
V_{cr}^W = & B_2^0 Y_{2,0}(\theta,\phi) + B_2^1(Y_{2,1}(\theta,\phi) - Y_{2,-1}(\theta,\phi)) \\
& + B_2^2(Y_{2,2}(\theta,\phi) + Y_{2,-2}(\theta,\phi)) \\
& + B_4^0(Y_{4,0}(\theta,\phi) + B_4^1(Y_{4,1}(\theta,\phi) - Y_{4,-1}(\theta,\phi)) \\
& + B_4^2(Y_{4,2}(\theta,\phi) + Y_{4,-2}(\theta,\phi)) \\
& + B_4^3(Y_{4,3}(\theta,\phi) - Y_{4,-3}(\theta,\phi)) \\
& + B_4^4(Y_{4,4}(\theta,\phi) - Y_{4,-4}(\theta,\phi)). \qquad (12)
\end{aligned}$$

The calculated CF parameters are listed in Table III, while the energy levels are presented in Fig. 5. Interestingly, the contribution of the exchange-charge parameters to the CF parameters is significantly higher than that of the point charges.

The spin-orbit interaction for the W^V ion can be written as

$$H_{SO} = \zeta_W \mathbf{ls}, \qquad (13)$$

where the spin-orbit parameter is $\zeta_W = 2500$ cm^{-1}. Our results imply that the common action of the CF and spin-orbit interaction results in a Kramers doublet ground state on each W^V ion. This Kramers doublet is well isolated from the excited levels, with a calculated energy gap of 19850 cm^{-1}. Therefore, the W^V ion can be described as a spin-$\frac{1}{2}$ with anisotropic g values which are $g_a^W = 1.595$, $g_b^W = 1.515$, and $g_c^W = 1.852$.

With the aid of Eqs. (6)–(10), we also deduced the CF potential for the Cu^{II} ions in the pentanuclear ligand surrounding of the WCuT compound (Fig. 1). The general

TABLE III. Crystal field parameters (in cm^{-1}) calculated for the W^V and Cu^{II} ions.

		B_2^0	B_2^1	B_2^2	B_4^0	B_4^1	B_4^2	B_4^3	B_4^4
W^V	Point	3279	3115	-2483	537	-795	-643	2563	-3128
	Exchange	7309	5257	-6002	6353	-9315	-7330	29 643	$-36\,360$
	Total	10 588	8372	-8485	6890	$-10\,110$	-7973	32 206	$-39\,488$
Cu^{II}	Point	-6572	1390	-210	1310	-110	29	33	-1328
	Exchange	$-11\,271$	1951	-188	13 764	-1379	303	316	$-15\,139$
	Total	$-17\,843$	3341	-398	15 074	-1489	332	349	$-16\,486$
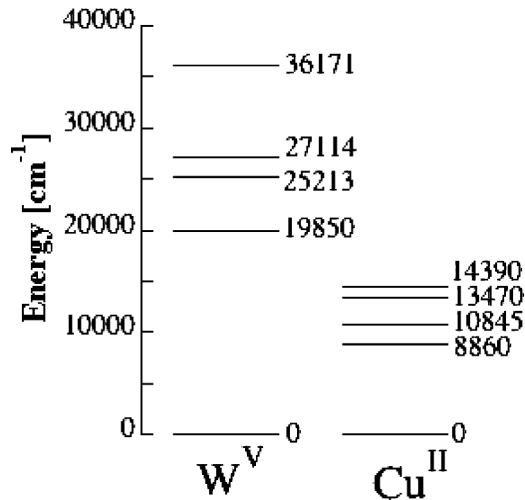
FIG. 5. Energy levels of the W^V and Cu^{II} ions calculated in the exchange-charge model of the CF with account of spin-orbital interaction.

form of this Hamiltonian coincides with that given in Eq. (12). For numerical estimation of the CF parameters for Cu^{II} we took the typical value $G = 8.1$, as determined from the data given in Refs. 38 and 39. The values of the CF parameters for copper are also given in Table III and the energy levels are presented in Fig. 5. It should be mentioned that the CF potentials for W and Cu ions are deduced for the same frame of reference. The introduction of spin-orbital interaction [$H_{SO} = \zeta_{Cu}\mathbf{ls}$, $\zeta_{Cu} = -830$ cm^{-1} (Ref. 40)] in the Hamiltonian for a single Cu^{II} leads to a Kramers doublet ground state separated from the first excited state by an energy gap of 8860 cm^{-1}. The local symmetry of the Cu ion is close to axial; the g-factor values are $g_a^{Cu} = 2.11$, $g_b^{Cu} = 2.10$, $g_c^{Cu} = 2.56$.

In summary, neglecting the spin-orbital interaction, we find that the ground states of W^V and Cu^{II} ions in the CF of the surrounding ligands are orbitally nondegenerate. In such a situation the first-order orbital angular momentum is quenched and local anisotropy may arise only by mixing of the ground and excited states by the spin-orbit interaction. For both ions the inclusion of spin-orbital interaction in the Hamiltonian leads to Kramers doublet ground states well separated from the excited states. The energy gaps between the ground and first excited Kramers doublets are 19 850 and 8860 cm^{-1} for the W^V and Cu^{II} ions, respectively. Though the gap is significantly smaller for copper, the spin-orbit interaction is stronger for tungsten (this is the general tendency for the $5d$ ions compared to the $3d$ ions[40]). As a consequence the contribution of the two ions to the local magnetic anisotropy is comparable, and the direction of the axial anisotropy of the g factors is the same (along c). Results of the CF calculations confirm that the values $g_b = 1.91$ and $g_c = 2.18$ deduced from the EMR experiment refer to a combined Cu/W excitation.

B. Band structure from DFT calculations

In order to understand better the electronic structure and the exchange paths in the WCuT system we performed spin-unrestricted DFT calculations with the program DMOL^3 (Ref. 41) using the Perdew-Becke-Enzerhof[42] correlation
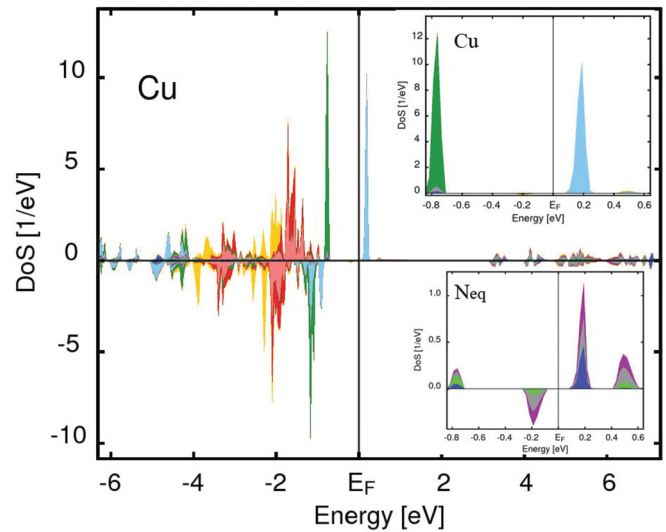
FIG. 6. (Color online) Partial density of states (pDOS) of copper. Contribution of the d_{y^2} orbitals is presented by the dark-green area, d_{xz} is shown in bright blue, $d_{x^2-z^2}$ in yellow, d_{xz} in blue, and d_{yz} in white-red. (Insets) Magnified regions near the Fermi level with pDOS of Cu (top right) and of the equatorial nitrogen (bottom right). The orbitals of the constituting N (shown) and C (not shown) atoms contribute to the same bands. Contributions of the s orbitals are shown in dark blue, p_x in violet, p_y in green, and p_z in gray.

functional. A lattice optimization was performed considering only the anionic layers, which were assigned the charge value of -4. The partial density of states (pDOS) of copper and tungsten presented in Figs. 6 and 7 implies that the d states are spread over a large energy range. These atoms also provide the bands near the Fermi level, which are partially occupied and are important for magnetic exchange. The gap between these bands and the higher energy unoccupied states is of the order of 3 eV, which is comparable to the sum of the gaps of the W^V ion
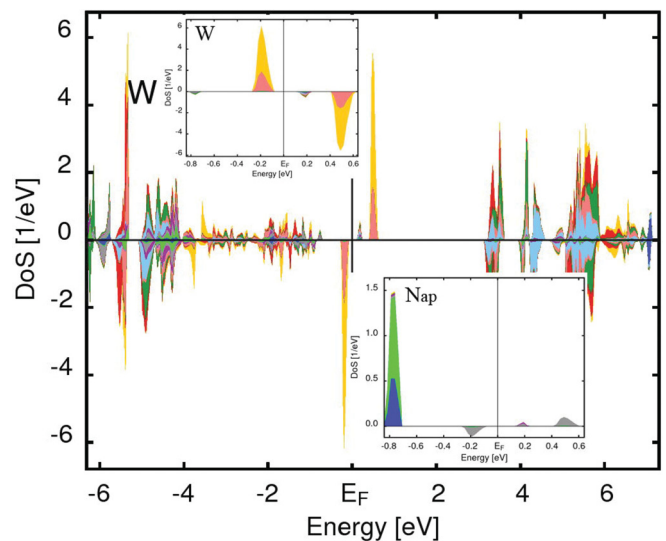
FIG. 7. (Color online) (Top) Partial density of states (pDOS) of tungsten. Magnified regions near the Fermi level with pDOS of W (top left) and of the apical nitrogen (bottom right). The color code of Fig. 6 is adopted.
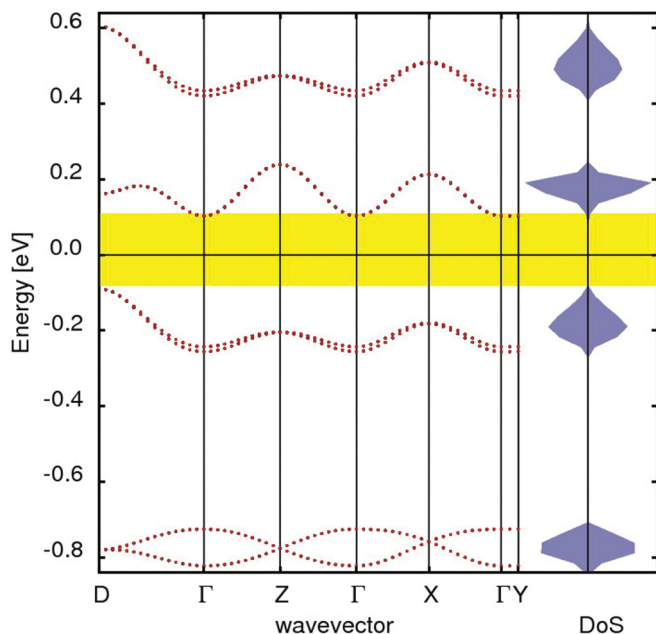
FIG. 8. (Color online) Band structure of WCuT along the selected symmetry directions in the Brillouin zone: $\Gamma = (0\ 0\ 0)$, $X = (\frac{1}{2}\ 0\ 0)$, $Y = (0\ \frac{1}{2}\ 0)$, $Z = (0\ 0\ \frac{1}{2})$, $D = (\frac{1}{2}\ 0\ \frac{1}{2})$. The majority and minority spin contributions are shown by black and red dotted lines, respectively.

and Cu^{II} ions predicted by the CF model ($28\,710\ cm^{-1} \approx 3.4\ eV$).

The bands near the Fermi level are rather narrow and show a dispersion in the ac layer, while in the b direction they are flat (Fig. 8). This fact supports the experimental findings that the magnetic exchange is strong in the ac plane and weak perpendicular to the layers. Notably, Figs. 6 and 7 show that the Cu and W orbitals contribute to different bands: those of copper contribute to the occupied valence band (VB) at -0.8 eV and to the lowest unoccupied conduction band (CB) at 0.2 eV, while those of tungsten dominate in the highest VB at -0.2 eV and in the CB at 0.5 eV. It is therefore reasonable to distinguish

the tungsten-CN and copper-CN orbital subsystems. From the shape and orientation of the Γ-point orbitals presented in Fig. 9 (left), the highest VB is dominated by the tungsten $5d_{x^2-z^2}$ and $5d_{yz}$ contributions and it is of the local π symmetry. The lowest CB (Fig. 9, right) is dominated by the copper $3d_{xz}$ orbitals and is of the local σ character. This implies mutual orthogonality of the two subsystems, which is the reason for the FM intra-bilayer interaction. This result is in agreement with DFT calculations for similar cyanide bridged compounds,[43,44] rationalizing them in terms of Kahn's model.[45,47]

Magnetic exchange between the W^V and Cu^{II} ions is of the superexchange nature and it is mediated mainly by the equatorial cyanide bridges (Fig. 1), which admix to all four bands (Fig. 6, bottom right). The unpaired electrons originating from the copper atoms partially delocalize into the equatorial nitrogen orbitals. This could be inferred from significant spin values at the equatorial nitrogens according to the Mulliken spin population analysis and also from the calculated spin-density distribution maps (Fig. 10). In contrast, the apical cyanide bridges contribute little to the magnetic exchange (Fig. 7, bottom right) and participate mainly to the occupied -0.8-eV band, which is involved in the chemical bonding. Thus, the equatorial and apical pathways provide different exchange efficiency, not because of orthogonality, but due to the small contribution of the apical cyanide orbitals to the magnetically active bands. This is most probably due to geometrical factors: the equatorial linkages are shorter [$d_{CuN} = 1.971(8)$ Å] and more bent [$\angle 169.3(7)°$, $\angle 169.4(8)°$], while the apical bridges are longer [2.115(7) Å] and less bent [$\angle 174(2)°$].[13] This difference could lead to different strengths of the apical J_{ap} and equatorial J_{eq} exchange couplings, but they would remain predominantly isotropic. To extract the exchange coupling constants within an isolated bilayer[46] we therefore used the Heisenberg Hamiltonian

$$H = J_{ap}(\mathbf{S}_1 \cdot \mathbf{S}_4 + \mathbf{S}_2 \cdot \mathbf{S}_3) + 4J_{eq}(\mathbf{S}_1 \cdot \mathbf{S}_3 + \mathbf{S}_2 \cdot \mathbf{S}_4) \quad (14)$$

for the exchange network of the WCuT unit cell. Here $\mathbf{S}_1$ and $\mathbf{S}_3$ are spin operators at the Cu and W sites of the same layer, while $\mathbf{S}_2$ and $\mathbf{S}_4$ are spin operators at the Cu and W sites of
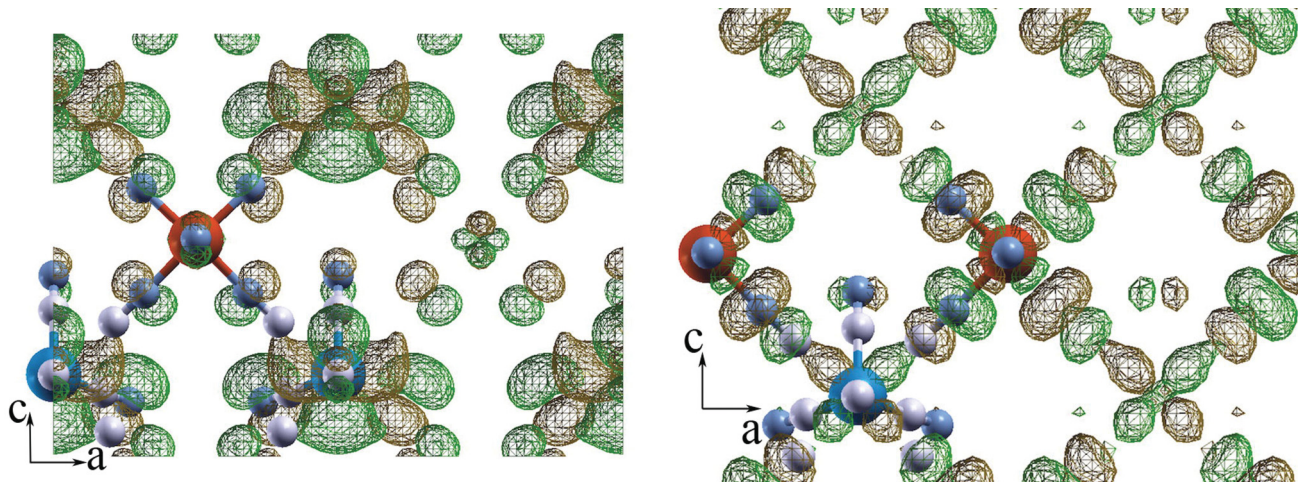
FIG. 9. (Color online) The ac projection of the single-layer Γ-point orbitals of the highest valence (left) and of the lowest conduction (right) bands. The color code of atoms of Fig. 1 is adopted. Green and brown isosurfaces correspond to two different signs of the orbitals.
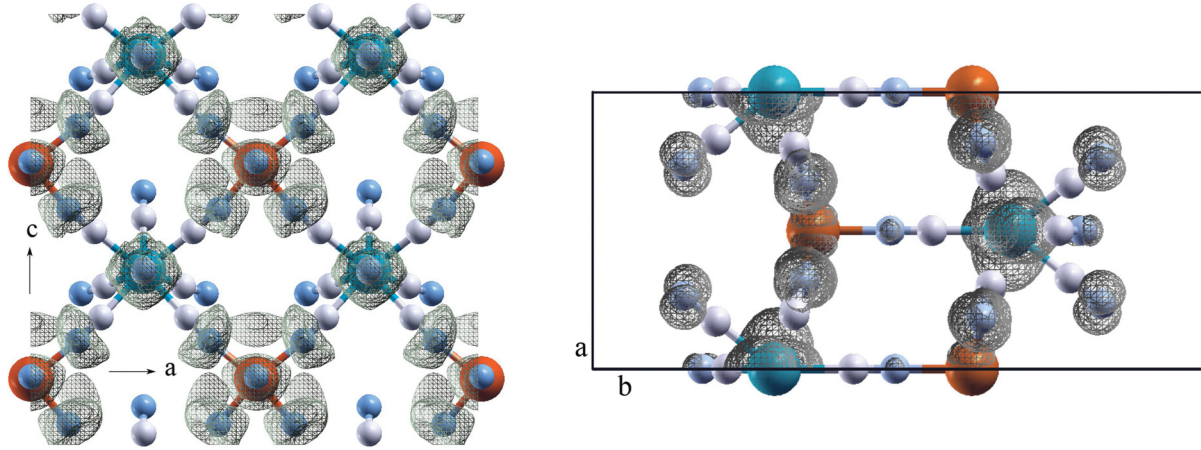
FIG. 10. (Color online) The *ac* (left) and *ab* (right) projections of the DFT spin density presented as gray isosurface.

the second layer of the bilayer. From DFT calculations we obtain that the ground-state configuration corresponds to the FM arrangement of spins in the bilayer, and configurations containing flipped spin(s) have higher energy. The exchange couplings estimated by comparing the energies of the ground and excited states are $J_{eq} = -8.5$ meV and $J_{ap} = -0.4$ meV. The experimental map presented in Fig. 4 corroborates partial delocalization of electron density on the equatorial nitrogens and the absence of such delocalization on the apical CN^- bridges. The collective exchange parameter zJ obtained by DFT ($-8.5 \times 4 - 0.4 = -34.4$ meV) results in the same estimate of the average intra-bilayer exchange coupling as given in Ref. 15 ($J = -77.5$ K $= -6.7$ meV).

C. Modeling of dipole-dipole interactions

M. Balanda *et al.* in Ref. 15 suggested that the inter-bilayer coupling in the WCuT system is of dipolar origin and that it is responsible for the stabilization of the 3D long-range order and for the metamagnetic behavior. To verify this picture we modeled the dipolar interactions by considering a sphere around a central ion i and calculated the energy of interaction of this ion with all other ions j within this sphere. The energy of the corresponding dipole-dipole interaction is

$$E_{dip} = \sum_j \frac{1}{r_{ij}^3} \left\{ \boldsymbol{\mu}_i \boldsymbol{\mu}_j - \frac{3(\boldsymbol{\mu}_i \mathbf{r}_{ij})(\boldsymbol{\mu}_j \mathbf{r}_{ij})}{r_{ij}^2} \right\}, \qquad (15)$$

where r_{ij} is the distance between the interacting W^V and Cu^{II} ions, and $\boldsymbol{\mu}$ are magnetic dipoles due to the electron spins,

$\boldsymbol{\mu}_i = -\mu_B \mathbf{g}_i \mathbf{S}_i$. We tried several configurations. The exchange coupling between the ions within the bilayers was always FM, but orientation of spins was chosen consecutively along the a, b, and c directions and the arrangement of moments of the neighboring bilayers was selected to be parallel or antiparallel. Also the two cases of isotropic and anisotropic g factors for both W^V and Cu^{II} ions were tested. In order to ensure the convergence of the calculations, spheres with the radius R up to 1000 Å were considered, and only results independent of the size are presented. The calculations listed in Table IV show that the minimum of the dipolar energy corresponds to AF alignment of the neighboring bilayers with individual spins aligned along the c direction. This is in accord with the magnetic structure determined by neutron diffraction. The calculated value of the external magnetic field which triggers magnetization reversal (Table IV) is also in good agreement with the experimental value (our magnetization data and Ref. 15).

We find it is crucial to take into account the anisotropy of the g factors. Figure 11 presents the dipolar energy as a function of the angle ϕ, which defines the tilt of spins from the c axis in the ac plane. In the case of isotropic g factors the spatial location of dipoles on the WCuT lattice (distances between the W^V and Cu^{II} ions) is the dominant factor defining the dipolar energy and thus favoring the spin alignment along the a axis (Fig. 11, curve 2), identical to the findings of Ref. 48. When anisotropic g factors (see Sec. III A) are taken into the consideration, this constituent of Eq. (15) prevails and the dipolar energy is minimal when the spins are oriented

TABLE IV. Energies of the configurations with FM (E_F) and AF (E_{AF}) bilayer couplings in the case of the spin alignment along the a, b, and c crystallographic directions for spheres of different radii R. Last column, the value of magnetic field corresponding to flip of the bilayers in the case of the spin alignment along the c direction.

R (Å)	$E_F \times 10^3$ (cm^{-1})			$E_{AF} \times 10^3$ (cm^{-1})			B_c (G)
	a	b	c	a	b	c	
50	−1.672	2.751	−1.763	−4.736	8.589	−6.238	52
100	−1.682	2.774	−1.783	−4.833	8.765	−6.365	53
200	−1.691	2.790	−1.795	−4.817	8.737	−6.345	53
1000	−1.750	2.141	−1.854	−4.808	8.744	−6.331	52
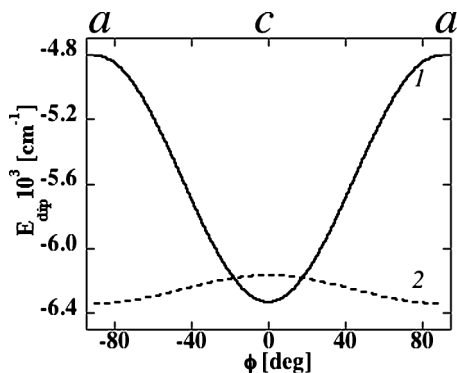
FIG. 11. The energy of dipole-dipole interaction as a function of the angle ϕ which shows the orientation of spins in the ac plane relative to the c direction in two cases: 1, with due account of the anisotropy of the g factors for Cu and W ions; 2, the g factors of both ions are isotropic.

along the c axis (Fig. 11, curve 1). The difference in energy between the antiferromagnetic and ferromagnetic configurations along the c direction per one ion is minute, equal to 0.0045 cm^{-1}; thus, a small magnetic field of 50 G applied along a is sufficient to initiate the metamagnetic transition.

In conclusion, dipolar interactions are indeed a very important constituent of the magnetic anisotropy in this compound. Modeling of the long-range magnetic ordering of the bilayers based on dipolar interactions and accounting for local (g factor) anisotropy of the constituent W^V and Cu^{II} ions reproduces the observed magnetic structure and the metamagnetic transition.

IV. DISCUSSION AND CONCLUSIONS

We studied magnetic anisotropy in the quasi-2D XY bilayered molecular magnet WCuT. A combination of experimental techniques—bulk magnetization measurements, EMR, neutron FR and neutron diffraction experiments on WCuT single crystals—indicates strong FM exchange coupling within the bilayers and significant magnetic anisotropy below 70 K. The b axis, normal to the layers, is the hard axis, while the anisotropy in the ac plane is small. Our EMR experiments clearly reveal static fields, which implies that strong 2D spin correlations are present at low temperatures, at least up to 70 K. This suggests that individual bilayers are ordered well above $T_C = 34$ K, resulting in the 2D behavior and the BKT nature of the transition, which were extensively studied in Refs. 16 and 17. Flipping ratios discriminate contributions of the W^V and Cu^{II} ions to the magnetic anisotropy and suggest that of W^V is more significant. The magnetic structure determined by neutron diffraction clarifies the details of the anisotropy within the easy plane; the magnetic moments are collinear and point along the c axis. Due to the weakness of magnetic intensities

the M_y magnetic component could not be determined, but it may exist as the Dzyaloshinsky-Moriya interaction is allowed by symmetry.

Our calculations within the exchange-charge single-ion CF model reveal that the ground states of both Cu^{II} and W^V are orbitally nondegenerate and these ions can be treated as possessing spin-$\frac{1}{2}$ and anisotropic g values. Magnetic anisotropy appears due to admixing of the ground state with the excited states by the spin-orbit interaction. The W^V ions have stronger spin-orbit coupling than Cu^{II}, but the gap between the ground and first excited states is lower for Cu^{II}. These two tendencies act against each other and, as a result, both ions contribute to the local magnetic anisotropy, which is along the c direction.

Our DFT calculations indicate that the bands near the Fermi level are predominantly of d character, with admixture of the cyanide states. The tungsten-CN and copper-CN orbital subsystems have different energies and different local symmetries: The first one dominates in the highest VB and has π symmetry; the second one constitutes the lowest CB and is of σ character. The orthogonality of these subsystems is most likely the reason for the dominant FM interaction in the system. The electronic structure obtained by DFT suggests that exchange paths in the ac plane of the single layer and the path along the b axis connecting layers into a bilayer are very different. The apical exchange path is less effective, as the hybridization between the orbitals of apical cyanides and the d orbitals of transition metals at the Fermi level is small. This leads to different equatorial and apical exchange couplings.

Calculation of the dipolar energy for various configurations indicate that the FM alignment of spins along the c direction with antiparallel coupling of moments at the neighboring bilayers is energetically favorable, but the minimal energy configuration is very dependent on anisotropy of the g factors. Our experimental and theoretical findings indicate that the combination of the local anisotropy of the g factors of the W^V and Cu^{II} ions and the long-range dipolar interactions on the ferromagnetically coupled squared bilayer WCuT lattice defines the XY-magnetic anisotropy and thus is responsible for the Kosterlitz-Thouless transition in the WCuT system.

[1]E. M. Motoyama, G. Yu, I. M. Vishik, O. P. Vajk, P. K. Mang, and M. Greven, Nature (London) **445**, 186 (2007).

[2]G. K. Campbell, Nat. Phys. **8**, 643 (2012).

[3]C. G. Smith, Rep. Prog. Phys. **59**, 235 (1996).

[4]L. V. Berezinskii, Zh. Eksp. Teor. Fiz. **59**, 907 (1970).

[5]J. M. Kosterlitz and D. J. Thouless, J. Phys. C **6**, 1181 (1973).

[6]M. Steiner, J. Villain, and C. G. Windsor, Adv. Phys. **25**, 87 (1976).

[7]L. de Jongh (ed.), *Magnetic Properties of Layered Transition Metal Compounds* (Kluwer, Dordrecht, 1990).

[8]Y. Endoh, K. Yamada, R. J. Birgeneau, D. R. Gabbe, H. P. Jenssen, M. A. Kastner, C. J. Peters, P. J. Picone, T. R. Thurston, J. M. Tranquada, G. Shirane, Y. Hidaka, M. Oda, Y. Enomoto, M. Suzuki, and T. Murakami, Phys. Rev. B **37**, 7443 (1988).

[9]H. Hirakawa and H. Ikeda, J. Phys. Soc. Jpn. **35**, 1328 (1973).

[10]H. Hirakawa and H. Yoshizawa, J. Phys. Soc. Jpn. **47**, 368 (1979).

[11]M. T. Hutchings, H. Ikeda, and E. Janke, Phys. Rev. Lett. **49**, 386 (1982).

[12]A. Palii, B. Tsukerblatt, J. M. Clemente-Juan, and E. Coronado, Int. Rev. Phys. Chem. **29**, 135 (2010).

[13]R. Podgajny, T. Korzeniak, M. Bałanda, T. Wasiutyński, W. Errington, T. J. Kemp, N. W. Alcock, and B. Sieklucka, Chem. Commun. 1138 (2002).

[14]T. Korzeniak, R. Podgajny, N. W. Alcock, K. Lewiński, M. Bałanda, T. Wasiutyński, and B. Sieklucka, Polyhedron **22**, 2183 (2003).

[15]M. Bałanda, T. Korzeniak, R. Pełka, R. Podgajny, M. Rams, B. Sieklucka, and T. Wasiutyński, Solid State Sci. **7**, 1113 (2005).

[16]F. L. Pratt, P. M. Zielinski, M. Balanda, R. Podgajny, T. Wasiutyński, and B. Sieklucka, J. Phys.: Condens. Matter **19**, 456208 (2007).

[17]M. Bałanda, R. Pełka, T. Wasiutyński, M. Rams, Y. Nakazawa, Y. Miyazaki, M. Sorai, R. Podgajny, T. Korzeniak, and B. Sieklucka, Phys. Rev. B **78**, 174409 (2008).

[18]A. Zorko, M. Pregelj, A. Potočnik, J. van Tol, A. Ozarowski, V. Simonet, P. Lejay, S. Petit, and R. Ballou, Phys. Rev. Lett. **107**, 257203 (2011).

[19]R. Podgajny, T. Korzeniak, K. Stadnicka, Y. Dromzée, N. W. Alcock, W. Errington, K. Kruczała, M. Bałanda, T. J. Kemp, M. Verdaguer, and B. Sieklucka, Dalton Trans. 3458 (2003).

[20]R. Podgajny, B. Sieklucka, and W. Łasocha, J. Chem. Soc., Dalton Trans. 1799 (2000).

[21]A. Gukasov and P. J. Brown, J. Phys.: Condens. Matter **14**, 8831 (2002).

[22]P. J. Brown, J. Phys. Chem. Solids **65**, 1977 (2004).

[23]H. Cao, A. Gukasov, I. Mirebeau, P. Bonville, C. Decorse, and G. Dhalenne, Phys. Rev. Lett. **103**, 056402 (2009).

[24]The choice of the principal directions was based on morphology of the crystal. One of the crystal faces was orthogonal to $a' = [0.95\ 0\ 0.31]$ ($20°$ tilt towards the c direction), rather then to a.

[25]P. J. Brown and J. C. Matthewman, Cambridge crystallography subroutine library—mark 4 (2000) http://www.ill.fr/dif/ccsl/html/ccsldoc.html.

[26]P. J. Brown, in *International Tables for Crystallography*, Vol. C Mathematical and Chemical Tables, Sec. 4.4.5, edited by A. J. C. Wilson (Kluwer, Dordrecht,1992), p. 391.

[27]B. Gillon, J. Larionova, E. Ruiz, Q. Nau, A. Goujon, F. Bonadio, and S. Decurtins, Inorg. Chim. Acta **361**, 3609 (2008).

[28]The off-diagonal λ_{bc} parameter could not be obtained reliably.

[29]F. Izumi and R. A. Dilanian, *Recent Research Developments in Physics* (Transworld Research Network, Trivandrum, 2002), Vol. 3, Part II, pp. 699–726.

[30]T. Moriya, Phys. Rev. **120**, 91 (1960).

[31]M. N. Popova, E. P. Chukalina, B. Z. Malkin, and S. K. Saikin, Phys. Rev. B **61**, 7421 (2000).

[32]S. Klokishner, O. Reu, S. Ostrovsky, A. Palii, and E. Towe, J. Phys.: Condens. Matter **19**, 486213 (2007).

[33]B. C. Gerstein, L. D. Thomas, and D. M. Silver, J. Chem. Phys. **46**, 4288 (1967).

[34]S. Klokishner, M. Behrens, O. Reu, G. Tzolova-Muller, F. Girgsdies, A. Trunschke, and R. Schlögl, J. Phys. Chem. A **115**, 9954 (2011).

[35]W. J. Hehre, R. F. Stewart, and J. A. Pople, J. Chem. Phys. **51**, 2657 (1969).

[36]E. Clementi and C. Roetti, At. Data Nucl. Data Tables **14**, 177 (1974).

[37]A. Nieuwpoort and J. Steggerda, Recl. Trav. Chim. Pays-Bas **95**, 289 (1976).

[38]B. J. Reddy, R. L. Frost, and W. N. Martens, Mineral. Mag. **69**, 155 (2005).

[39]F. Rodriguez, A. G. Bredosat, J. A. Aramburu, M. Morenot, and J. M. Calleja, J. Phys. C **20**, 641 (1987).

[40]A. Abragam and B. Bleaney, *Electron Paramagnetic Resonance of Transition Ions* (Clarendon, Oxford, 1970).

[41]B. J. Delley, J. Chem. Phys. **92**, 508 (1990).

[42]J. P. Perdew, K. Burke, and M. Ernzerhof, Phys. Rev. Lett. **77**, 3865 (1996).

[43]R. Podgajny, R. Pełka, C. Desplanches, L. Ducasse, W. Nitek, T. Korzeniak, O. Stefańczyk, M. Rams, B. Sieklucka, and M. Verdaguer, Inorg. Chem. **50**, 3213 (2011), and references therein.

[44]T. Korzeniak, C. Desplanches, R. Podgajny, C. Gimenez-Saiz, K. Stadnicka, M. Rams, and B. Sieklucka, Inorg. Chem. **48**, 2865 (2009).

[45]O. Kahn, *Molecular Magnetism* (VCH, New York, 1993), Chap. 8.4.2.

[46]We obtained equal energy for the DFT configurations with the F and AF alignment of the bilayers.

[47]This model considers the exchange coupling J as the sum of the ferro- J_F and antiferro- J_{AF} couplings, with $J_F = 2k$ and $J_{AF} = 4\beta s$. Here k is the two-electron exchange integral, β is the one-electron resonance integral, and s the one-electron overlap integral.

[48]S. Kaneko, Y. Tsunobuchi, S. Sakurai, and S. Ohkoshi, Chem. Phys. Lett. **446**, 292 (2007). To avoid confusion we mention that the a, b, and c axes of WCuT correspond to the c, a, and b axes of the compound discussed in this reference.